JOC The Journal of Organic Chemistry

Article

pubs.acs.org/joc

# Subtle Chemical Shifts Explain the NMR Fingerprints of Oligomeric Proanthocyanidins with High Dentin Biomodification Potency

Joo-Won Nam,[†] Rasika S. Phansalkar,[†] David C. Lankin,[†] Jonathan Bisson,[†] James B. McAlpine,[†,‡] Ariene A. Leme,[§] Cristina M. P. Vidal,[§] Benjamin Ramirez,[∥] Matthias Niemitz,[⊥] Ana Bedran-Russo,[§] Shao-Nong Chen,[†,‡] and Guido F. Pauli*[,†,‡]

[†]Department of Medicinal Chemistry & Pharmacognosy, [‡]Institute for Tuberculosis Research, College of Pharmacy, [§]Department of Restorative Dentistry, College of Dentistry, and [∥]UIC Center for Structural Biology, University of Illinois at Chicago, Chicago, Illinois 60612, United States

[⊥]PERCH Solutions Ltd., Puijonkatu 24 B 5, 70110 Kuopio, Finland

Supporting Information

**ABSTRACT:** The ability of certain oligomeric proanthocyanidins (OPACs) to enhance the biomechanical properties of dentin involves collagen cross-linking of the 1.3−4.5 nm wide space via protein−polyphenol interactions. A systematic interdisciplinary search for the bioactive principles of pine bark has yielded the trimeric PAC, *ent*-epicatechin-(4$\beta$→8)-epicatechin-(2$\beta$→*O*→7,4$\beta$→8)-catechin (**3**), representing the hitherto most potent single chemical entity capable of enhancing dentin stiffness. Building the case from two congeneric PAC dimers, a detailed structural analysis decoded the stereochemistry, spatial arrangement, and chemical properties of three dentin biomodifiers. Quantum-mechanics-driven $^{1}$H iterative full spin analysis (QM-HiFSA) of NMR spectra distinguished previously unrecognized details such as higher order *J* coupling and provided valuable information about 3D structure. Detection and quantification of H/D-exchange effects by QM-HiFSA identified C-8 and C-6 as (re)active sites, explain preferences in biosynthetic linkage, and suggest their involvement in dentin cross-linking activity. Mapping of these molecular properties underscored the significance of high $\delta$ precision in both $^{1}$H and $^{13}$C NMR spectroscopy. Occurring at low- to subppb levels, these newly characterized chemical shift differences in ppb are small but diagnostic measures of dynamic processes inherent to the OPAC pharmacophores and can help augment our understanding of nanometer-scale intermolecular interactions in biomodified dentin macromolecules.

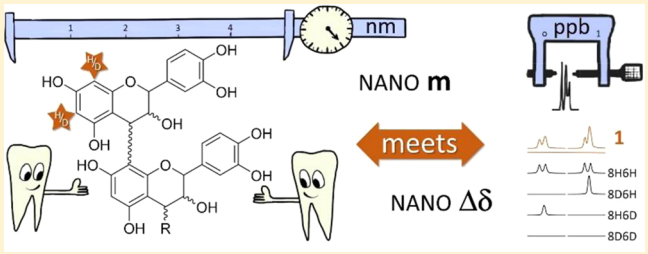


## INTRODUCTION

Structural modification of dentin with natural products, that is, biomodification, is an emerging means of enhancing the biomechanical properties and biostability of dentin, the peptidic core of the human tooth, and thereby advancing restorative dentistry. Dentin is a complex mineralized tissue, mainly composed of type I collagen and other noncollagenous proteins such as phosphoproteins and proteoglycans.[1] Recently, our interdisciplinary program has shown that certain plants, such as pine (*Pinus massoniana* LAMB., Pinaceae) produce specific condensed tannins with high dentin matrix bioactivity.[2] Pine bark is a promising source of such polyphenols: oligomeric proanthocyanidins (OPACs), which are condensation products of flavan-3-ols and form an analytically complex group of congeners (see refs 3,4 for a summary of the nomenclature). Dentin biomodification involves the establishment of non-enzymatic collagen cross-linkages mediated by OPACs. From a spatial perspective, selective OPACs act at the nanometer scale, bridging collagen inter-molecularly and inter-microfibrillarly in the 1.3−4.5 nm range.[5]

While the antioxidant,[6] anti-inflammatory,[7] antimicrobial,[8,9] and anticancer[10] effects are frequently reported among the rather broad biological properties of OPACs, we are only beginning to understand how OPACs can act specifically by enhancing the biomechanics of dentin via collagen cross-linking.[4,11] Three key chemical prerequisites for the study of the intermolecular interactions between dentin and the bioactive OPACs can be identified: (a) purification of the dentin-bioactive OPACs from the complex natural matrix and in their genuine form, as they occur in the plant; (b) comprehensive chemical characterization of the oligomers, again in their underivatized form, and including the relative and absolute configuration of the [*epi*-]/[*ent*-]catechin subunits; and (c) information about their 3D structures, including the atropisomeric rotamers and other dynamic phenomena known to occur in aqueous solutions such as H exchange. Affecting both (b) and (c), one intriguing chemical question for trimers and higher oligomers is about the linkage type(s) and sites of the

**Received:** May 14, 2015
**Published:** July 27, 2015





DOI: 10.1021/acs.joc.5b01082
J. Org. Chem. 2015, 80, 7495−7507

individual monomers as being B-type (single C−C interflavanyl bond) and/or A-type (C−C and C−O−C doubly linked interflavanyl bond). Notably, the OPAC portion of the tannin metabolome ("tannomes") in any given plant can exhibit an enormous number of structural variations due to the different constituting monomers, linkage types and sites, and as a function of the degree of polymerization (DP). Accordingly, on the basis of our current knowledge of the PAC chemistry in pine bark (four monomeric units; seven linkage type/site variations), over 3000 theoretical PAC structures of trimers alone exist in this plant.[5]

The intrinsic connections between all three points (a/b/c) rationalize the challenges associated with the structure elucidation and reproducible supply of pure compounds for biomechanical studies. This also explains why the chromatographic and NMR spectroscopic literature on free-phenolic OPACs is scarce and rather fragmentary, and why advanced analytical methodology addressing a/b/c is in high demand. The $^{1}$H and $^{13}$C NMR spectra of PACs consisting of congeneric monomers, that is, the stereoisomeric catechins, show heavily overlapped signals due to the lack of dispersion, even at high fields. Moreover, many 1D and 2D NMR spectra of PACs are hardly interpretable at room temperature, exhibiting very broad lines or even "missing" resonances due to molecular dynamics, particularly atropisomerism and exchange (c).[12] To overcome these limitations, our approach uses a combination of low temperature NMR, quantum-mechanical driven $^{1}$H iterative full spin analysis (QM-HiFSA), and QM-HiFSA-based analysis of H/D-exchange to unequivocally characterize dentin-bioactive OPACs (**1**−**3**) from pine bark (Scheme 1).

**Scheme 1. Structures of the Oligomeric Proanthocyanidins (OPACs) A1 (1), A2 (2), and *ent*-Epicatechin-(4$\beta$→8)-epicatechin-(2$\beta$→*O*→7,4$\beta$→8)-catechin (3)**[a]

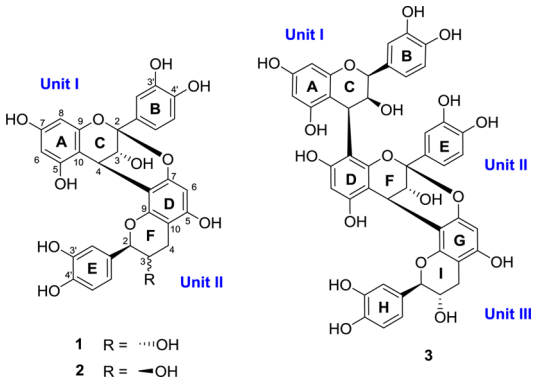


[a]Each unit (I−III) represents a monomeric building block of **1**−**3**.

The outcome shows that chemical shifts and substituent chemical shift effects (SCSs) measured at the ppb level ($\delta$ and $\Delta\delta$, respectively, rather than expressed in ppm) are meaningful properties in the analysis of their $^{1}$H and $^{13}$C solution NMR spectra. As structural properties of bioactive OPACs in solution are encoded into these ppb-level chemical shifts, their recognition becomes relevant for the understanding of how select OPACs are able to act as cross-linkers not only intermolecularly, but also in the inter-microfibrillar space of dentin, both occurring at the nanometric range.[5,11] This instance of "nano meets nano" connects previously unrecognized, very subtle substituent chemical shifts effects (SCSs; $\Delta\delta$s, expressed in ppb) with the structural characteristics of OPACs that exhibit the "perfect fit" at the nanometer level, allowing them to interact most efficiently with the dentin matrix within its highly complex hierarchy. Notably, OPAC **3** is the most potent single chemical entity with dentin stiffness enhancing activity, purified to date (see Results and Discussion). Moreover, the size of this trimeric PAC matches the spatial dimension hypothesis of high-potency cross-linking agents developed recently.[5,11]

To address requirement (a), we have developed multistep chromatographic protocols that employ orthogonal separation techniques to yield free-phenolic OPACs of purity adequate for biological assessment (typically >95% by qHNMR, calcd as the sum of rotamers). Addressing aspects of both (b) and (c), the mining of the rich structural information encoded in the form of $\delta$ and $J$ in the 1D $^{1}$H and $^{13}$C NMR spectra was initiated by performing an unequivocal signal assignment, aided by low temperature 2D NMR. Subsequent QM-HiFSA of **1**−**3**, paired with resolution enhanced $^{13}$C NMR spectra, was instrumental in distinguishing the level of spectral detail that enabled a full understanding of the observed "multiplets" and, importantly, revealed the underlying molecular properties that otherwise remain inaccessible by visual interpretation.

The net outcome is a gain in the understanding of the atropisomeric species that contribute to the rotameric dynamics, the identification of the absolute configurations of the [*epi*-]/[*ent*-]catechin building blocks, and the ability to not only pinpoint the C-6 and C-8 methine protons as being prone to H exchange,[13−15] but also to assess the exchange quantitatively on the basis of the associated ppb-level SCS effects. This finding has biosynthetic implications as both carbons represent the key sites for interflavanyl C−C linkages. Different H−D exchange rates reflect the electron density differences at both carbons, triggered by the acidity of the A-ring hydroxy groups (5-/7-OH). Furthermore, **1**−**3** provide evidence that enhanced ppb-level precision is applicable not only to the $^{1}$H domain of NMR,[16] but also to $^{13}$C NMR data. This study demonstrates that the $^{1}$H NMR spectra of OPACs can be fully understood using the HiFSA approach, by considering them as being mixtures of multiple species per molecule. Concurrently, this provides unprecedented confidence for the identification and rapid dereplication of congeneric compounds by routine 1D $^{1}$H NMR.

Collectively, the findings pave the way for mechanistic studies of the biomolecular interactions responsible for the specific ability to enhance the dentin modulus of elasticity of certain OPAC molecules.

## RESULTS AND DISCUSSION

**Isolation of Pine PACs (1−3).** Three PACs, proanthocyanidin A1 (**1**), A2 (**2**), and *ent*-epicatechin-(4$\beta$ → 8)-epicatechin-(2$\beta$→*O*→7,4$\beta$→8)-catechin (**3**), were isolated from the inner barks of *P. massoniana*. As PACs, they showed reddish coloration after spraying TLC plates with vanillin-sulfuric acid reagent, a color reaction that is characteristic of proanthocyanidins.[17] The structures of isolated compounds were determined by a combination of $^{1}$H iterative full spin analysis (HiFSA) in addition to HRESIMS, ECD, 1D, and 2D NMR spectroscopy. The qHNMR purities (%, w/w) of the isolated compounds **1**−**3** were 95.3%, 99.8%, and 95.4%, respectively, determined by the 100% method (S1−S3, Supporting Information).[18]

**Assignment of $^{1}$H and $^{13}$C Resonances of Dimers 1 and 2.** The NMR spectra of PACs are easily misinterpreted due to their conspicuous similarities. $^{1}$H NMR signals of PACs


DOI: 10.1021/acs.joc.5b01082
J. Org. Chem. 2015, 80, 7495−7507

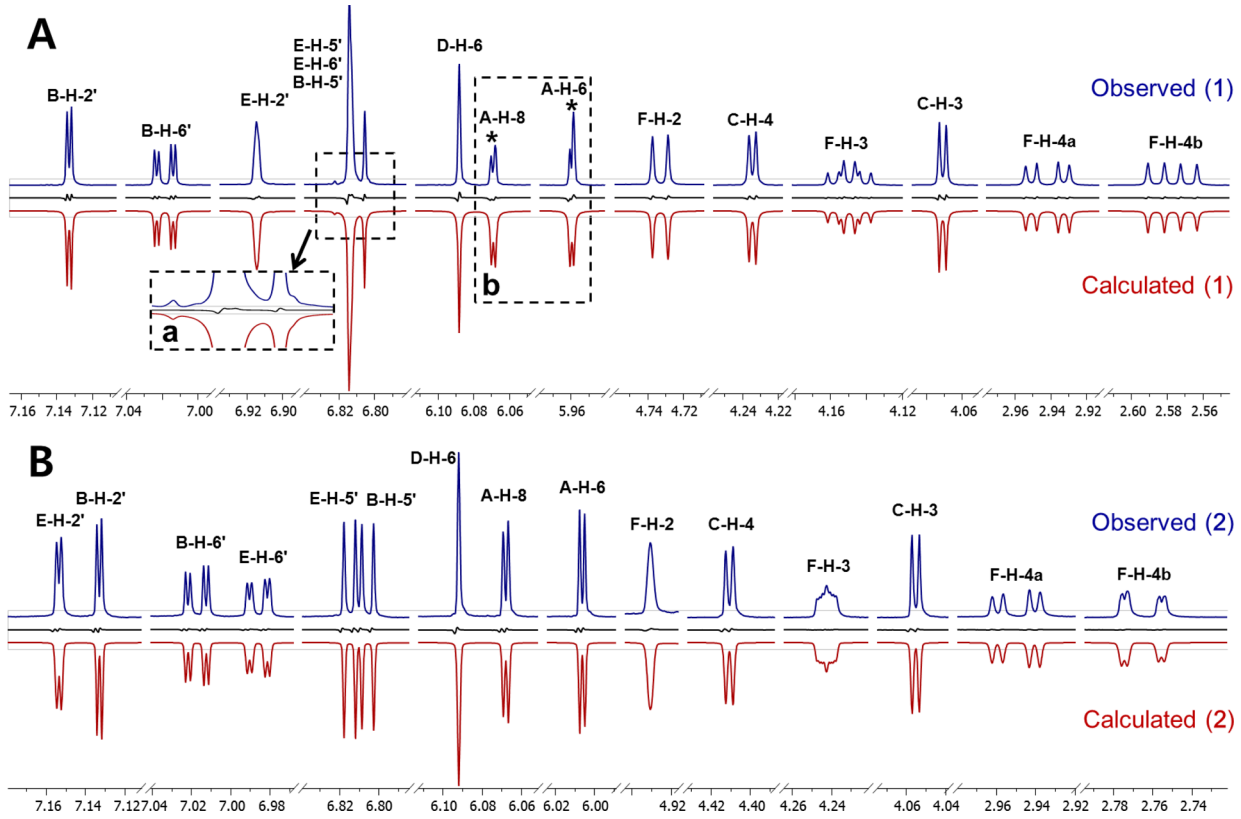


**Figure 1.** $^{1}$H NMR fingerprints of compounds **1** (A) and **2** (B) generated by HiFSA. Comparison of the observed (blue, obtained in $CD_3OD$ at 900 MHz, 298 K) and calculated (red) $^{1}$H spectra, including residuals in black. Asterisks (*) denote the relatively poorly matched region (local RRMS = 0.350), resulting from proton−deuterium exchange effects in the A-ring after storage in $CD_3OD$ for 4 months at −20 °C.

are highly complex because of signal overlaps caused by repetition of similar monomeric units. Initial attempts to identify the structures of **1** and **2** via comparison of experimental with reported NMR data pointed to inconsistencies of assignments reported for the aromatic protons.[19−22] In fact, an ab initio approach including unambiguous and precise assignment of all $^{1}$H and $^{13}$C NMR resonances as well as establishment of $^{1}$H NMR fingerprints was required to achieve the structural identification of **1** and **2** as follows (S4−S9, Supporting Information).

The molecular formulas of compounds **1** and **2** were determined by HR-ESI−MS to be $C_{30}H_{24}O_{12}$, indicating **1** and **2** to be doubly linked dimeric procyanidins. The existence of 2→*O*→7 and 4→8 doubly linked interflavanyl bonds in **1** and **2** was confirmed by HMBC cross peaks from H-4 (C-ring) to C-7, C-8, and C-9 (D-ring). These connections were further confirmed by the $^{13}$C chemical shift of C-8 ($\delta_C$ 106.77, **1**; $\delta_C$ 107.21, **2**) in the D ring, as the C-8 chemical shift (ca. $\delta_C$ 107.0) of 2→*O*→7/4→8 linked structures can be distinguished from the C-6 chemical shift (ca. $\delta_C$ 108.8) of 2→*O*→7/4→6 linked structures.[20] The relative configurations of H-2/H-3 (F-ring) of the lower unit in **1** and **2** were established as *trans* (catechin) and *cis* (epicatechin), respectively, by comparing the $^{1}$H coupling constants ($^{3}J_{2H,3H}$ = 7.88 Hz, **1**; $^{3}J_{2H,3H}$ < 2 Hz, **2**). The absolute configurations at C-4 (C-ring) in **1** and **2** were determined by ECD spectra (S10, Supporting Information). Positive and negative Cotton effects in the region of 220−240 nm indicated 4$\beta$ and 4$\alpha$ orientations of the flavan-3-ol groups, respectively.[23,24] The 4$\beta$ orientation and, hence, 4*R* absolute configurations of **1** and **2** were determined by strong positive Cotton effects ($\Delta\varepsilon$ = +28.58, **1**; $\Delta\varepsilon$ = +33.63, **2**) at 223 nm. Further analysis of the $^{1}$H NMR, DEPTQ-135, COSY, HSQC, and HMBC NMR data as well as comparison with authentic samples led to full assignments of the $^{1}$H and $^{13}$C NMR resonances and unambiguously confirmed their identity as the known proanthocyanidins A1 and A2,[20] respectively (S11, Supporting Information).

**Generation of $^{1}$H NMR Fingerprints of Compounds 1 and 2.** It is highly recommended that chemical shifts ($\delta$ values) and coupling constants ($J$ values) should be reported with at least 1 ppb (better 0.1 ppb) and 10 mHz precision, respectively.[16] To facilitate future structure dereplication of congeneric proanthocyanidins, precise $^{1}$H NMR profiles of **1** and **2** were generated by HiFSA[25,26] using the PERCH software tools. After 3D molecular structures were prepared in the MMS module, initial $^{1}$H spin parameters ($\delta_H$, $^{n}J_{H,H}$, and $\Delta\nu_{1/2}$) were predicted and then optimized by quantum mechanical simulation of the spectra in the PERCH iterator using D and T modes for integral-transform fitting and total-line shape fitting, respectively. The iteration was repeated until the root-mean-square (RMS) values were <0.1 (RMS = 0.050 for **1**; RMS = 0.067 for **2**), indicating excellent agreement between simulation results and observed data (Figure 1). The true $^{1}$H spin parameters (Table 1) were thus determined with high precision of chemical shifts ($\delta_H$ 0.1 ppb) and coupling constants ($J$, 10 mHz).

In general, the HiFSA approach enables the assignment of all $^{1}$H NMR resonances, including those that cannot be interpreted by visual interpretation and/or involve small long-range couplings ($J$ < 2 Hz). Importantly, HiFSA established the *ortho* benzylic couplings ($^{4}J_{E\text{-}H\text{-}2',\ F\text{-}H\text{-}2}$) of **1** and **2** as being −0.55 and −0.33 Hz, respectively (Figure 2). Benzylic



DOI: 10.1021/acs.joc.5b01082
J. Org. Chem. 2015, 80, 7495−7507

Table 1. Comprehensive $^{1}H$ and $^{13}C$ NMR Spectroscopic Data of Compounds 1 and 2[a,b]

| | position | 1 $\delta_H$ ($J$, Hz) | 2 $\delta_H$ ($J$, Hz) |
|---|---|---|---|
| unit I | | | |
| C | 3 | 4.0710, d (3.43) | 4.0553, d (3.31) |
| | 4 | 4.2343, d (3.43) | 4.4108, d (3.31) |
| A | 6 | 5.9591, d (2.32)[d] | 6.0065, d (2.32) |
| | 8 | 6.0688, d (2.32)[d] | 6.0681, d (2.32) |
| B | 2′ | 7.1329, dd (2.18, <0.10[c]) | 7.1332, dd (2.14, <0.10[c]) |
| | 5′ | 6.8101, dd (8.23, <0.10[c]) | 6.8075, dd (8.28, <0.10[c]) |
| | 6′ | 7.0183, dd (8.23, 2.18) | 7.0173, dd (8.28, 2.14) |
| unit II | | | |
| F | 2 | 4.7328, dd (7.88, −0.55) | 4.9311, dd (1.38, −0.33) |
| | 3 | 4.1495, ddd (8.25,7.88, 5.57) | 4.2426, ddd (4.85, 2.76, 1.38) |
| | 4 | 2.9414, dd (−16.36, 5.57) | 2.9500, dd (−16.99, 4.85) |
| | | 2.5772, dd (−16.36, 8.25) | 2.7658, dd (−16.99, 2.76) |
| D | 6 | 6.0879, s | 6.0921, s |
| E | 2′ | 6.9145, ddd (2.10, −0.55, <0.10[c]) | 7.1538, ddd (2.08, −0.33, <0.10[c]) |
| | 5′ | 6.8147, dd (8.13, <0.10[c]) | 6.8134, dd (8.13, <0.10[c]) |
| | 6′ | 6.8122, dd (8.13, 2.10) | 6.9861, dd (8.13, 2.08) |

| | position | 1 $\delta_C$, mult. | 2 $\delta_C$, mult. | | position | 1 $\delta_C$, mult. | 2 $\delta_C$, mult. |
|---|---|---|---|---|---|---|---|
| unit I | | | | unit II | | | |
| C | 2 | 100.29, C | 100.17, C | F | 2 | 84.49, CH | 81.77, CH |
| | 3 | 67.79, CH | 68.10, CH | | 3 | 68.09, CH | 67.01, CH |
| | 4 | 29.20, CH | 29.27, CH | | 4 | 29.00, $CH_2$ | 29.93, $CH_2$ |
| A | 5 | 156.73, C[d] | 157.02, C | D | 5 | 156.13, C | 156.62, C |
| | 6 | 98.13, CH | 98.28, CH | | 6 | 96.51, CH | 96.46, CH |
| | 7 | 158.12, C[d] | 158.14, C | | 7 | 152.18, C | 152.32, C |
| | 8 | 96.51, CH | 96.60, CH | | 8 | 106.77, C | 107.21, C |
| | 9 | 154.21, C[d] | 154.25, C | | 9 | 151.40, C | 152.15, C |
| | 10 | 104.00, C | 104.24, C | | 10 | 103.10, C | 102.40, C |
| B | 1′ | 132.28, C | 132.46, C | E | 1′ | 130.53, C | 131.21, C |
| | 2′ | 115.59, CH | 115.60, CH | | 2′ | 115.74, CH | 116.01, CH |
| | 3′ | 146.76, C | 145.67, C | | 3′ | 146.76, C | 146.01, C |
| | 4′ | 145.63, C | 146.77, C | | 4′ | 146.32, C | 146.31, C |
| | 5′ | 116.30, CH | 115.92, CH | | 5′ | 115.67, CH | 115.65, CH |
| | 6′ | 119.81, CH | 119.77, CH | | 6′ | 120.67, CH | 120.34, CH |

[a]The $^{1}H$ and $^{13}C$ NMR data were acquired in $CD_3OD$ at 900 and 225 MHz, respectively. [b]The $\delta_H$ (in ppm) and $J$ (in Hz) values were determined by $^{1}H$ iterative full spin analysis (HiFSA). [c]Very small couplings were detected by HiFSA and required for the overall fit. [d]Chemical shifts and coupling constants of nondeuterated species (6H8H).

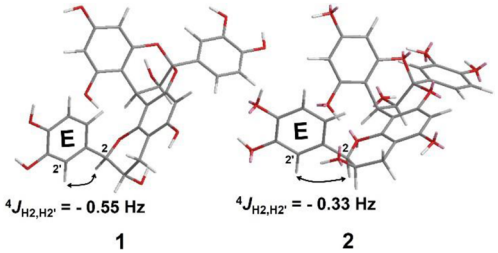


**Figure 2.** Diagnostic *ortho* benzylic long-range couplings ($^{4}J_{HH}$) in compounds **1** and **2**.

couplings exist between benzyl protons and *ortho*/*meta*/*para* protons of adjacent aromatic rings, resulting from the $\sigma-\pi$ configuration interaction mechanism.[27] The *ortho* benzylic couplings are related to allylic couplings and are generally associated with negative $J$ values.[27,28] These couplings likely contribute to peak broadening, even if they are not visually detectable in the spectrum, but can be extracted and their size determined via HiFSA.

**Higher Order Effects in the $^{1}H$ NMR Spectrum of Compound 1.** As shown in Figure 1A (a), the $^{1}H$ NMR resonances for H-2′, 5′, and 6′ of the E-ring exhibited higher order "multiplets", an assignment that can lead to misinterpretation of the spectrum. Evidently, the signals did not show the typical AMX splitting patterns, due to higher order effects resulting from close resonance frequencies of two highly coupled protons, E-H-5′ and E-H-6′. This effect depends on the ratio of chemical shift differences ($\Delta\delta$) and magnitudes of coupling constants ($J$) of the corresponding spin systems.[29] Conventional determination of $J$ and $\delta$ values by manual measurement of line distances and determination of peak centers can lead to misinterpretation by neglecting higher order effects. However, spectral simulation, such as performed as part of HiFSA, is a prerequisite for obtaining precise $J$ and $\delta$ values, especially from non-first-order spin systems. Figure 3 shows that the apparent d and dd multiplicities for the AMX signals of E-H-5′ and E-H-6′, respectively, disappear at $\Delta\delta$ values of <9



DOI: 10.1021/acs.joc.5b01082
J. Org. Chem. 2015, 80, 7495−7507

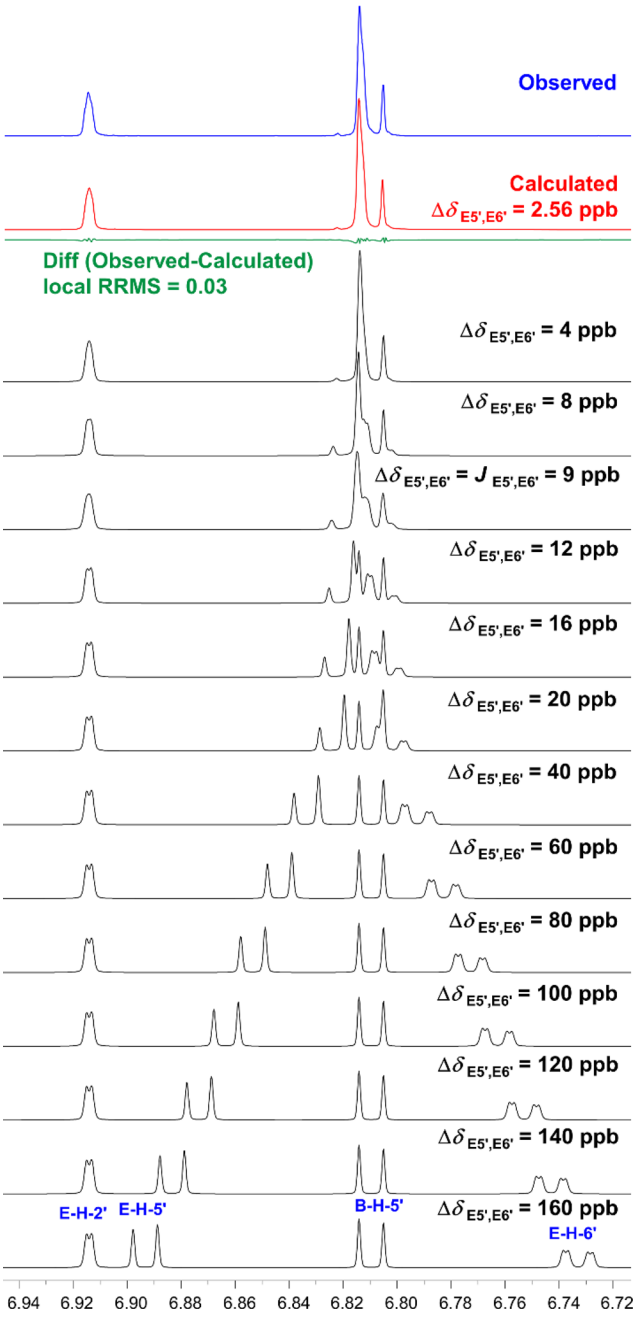


**Figure 3.** Demonstration of the higher order effect of the resonances of E-H-2′, E-H-5′, and E-H-6′ in **1**, caused by the close resonance behavior ($\Delta\delta$ = 2.56 ppb) of the E-5′ and E-6′ protons. The AMX spin system changes to the AXY spin system upon decreasing $\Delta\delta$ (E-H-5′, E-H-6′) from 160 to 2.56 ppb. Shown are simulated spectra for various values of $\Delta\delta$ (E-H-5′, E-H-6′; 900 MHz; simulation performed with the PERCH software tool). An animated graphic (GIF media file) of the transitions shown here is provided as Supporting Information.

ppb (~8 Hz at 900 MHz), which is equivalent to the $J_{E5',E6'}$ coupling.

Decreasing $\Delta\delta$ further causes all signals of the emerging AXY spin system to degrade to a complex, broadened set of resonances, with no resemblance to the multiplicity that could be inferred on the basis of first-order assumptions. Importantly, the chemical shifts are no longer "located" in the center of the signals. As the chemical shifts of two protons get closer, the intensity ratio of outer (O) to inner (I) lines of the resonance

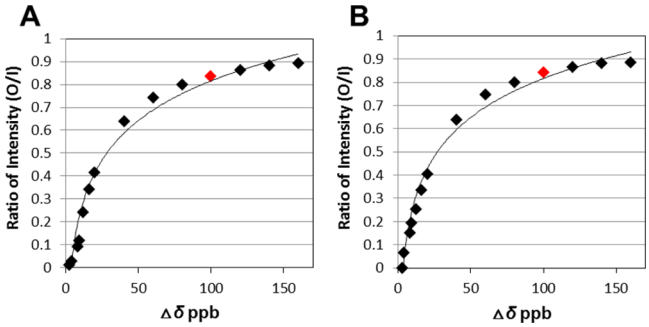


**Figure 4.** Correlations between $\Delta\delta$ and the intensity ratio of the outer (O) to the inner lines (I) of E-H-5′ (A) and E-H-6′ (B) (black ◆). The red ◆ represents the case of $\Delta\delta_{E5',E6'}$ coinciding with $J_{E5',E6'}$ = 8.13 Hz (9 ppb at 900 MHz).

patterns gets smaller (Figure 4). The signal from E-H-2′, although not a highly coupled proton with either E-H-5′ or E-H-6′, also begins to show triplet-like peak shape, due to virtual coupling caused by a higher order effect when $\Delta\delta_{E5',E6'}$ is the same as $J_{E5',E6'}$. The top trace in Figure 3 showing the HiFSA result explains why a first-order assumption applied to the interpretation of an apparently "simple" aromatic spin system, such as the AMX-type B-ring in PACs, can be misleading and prevents proper identification of the partial structure and/or entire molecule. Collectively, this shows that SCS effects perceived as being minor (e.g., 2 Hz = 2.2 ppb at 900 MHz) can have profound effects on the observed signal pattern arising from near-identical molecules. Examples of such effects are numerous and can include solvent effects, magnetic field effects, concentration effects, temperature effects, aromatic solvent-induced shift (ASIS) effects, and conformational effects.[30] As demonstrated above, computer-assisted spectral analysis is essential for the interpretation of the $^1$H spectra by extracting precise spectral parameters.

**Hydrogen and Deuterium Exchange Causes ppb-Level Chemical Shift Differences in the A-Ring of Proanthocyanidins.** The total RMS of 0.050 (<0.1), the HiFSA result, and the close visual match (Figure 1A) indicated excellent agreement between the experimental and calculated spectra of **1**. However, when looking more closely, unacceptable differences in certain spectral regions (5.95−6.08 ppm, Figure 1A (b)) with local RRMS (regional RMS) values of 0.350 (>0.1) were observed. In this region, the A-ring H-6 and H-8 resonances showed signals with reduced intensity and without a "roof effect" as would be expected for signals of strongly coupled partners, pointing at each other. This results from a H/D exchange reaction of flavonoids ([O]PACs and anthocyanidins), occurring in solution in deuterated protic solvents, such as $CD_3OD$ or $D_2O$.[13−15,31] Under acidic conditions (e.g., $CF_3COOD$), H/D exchange reactions of phenolic hydrogens occur rapidly, over seconds to minutes, via keto−enol tautomerization or electrophilic-substitution reaction.[31−33] On the other hand, under neutral conditions, H/D exchange takes from several hours to days (S12, Supporting Information),[14,34] and recent evidence shows that amines (e.g., [hydroxy-]lysine in collagen) can facilitate deuteration under very mild conditions.[35] In the present study, the H/D exchange process of **1** dissolved in $CD_3OD$ could be followed over time in the 1D NMR spectra. Observed differences in H/D exchange rates are caused by electron density differences associated with


DOI: 10.1021/acs.joc.5b01082
J. Org. Chem. 2015, 80, 7495−7507

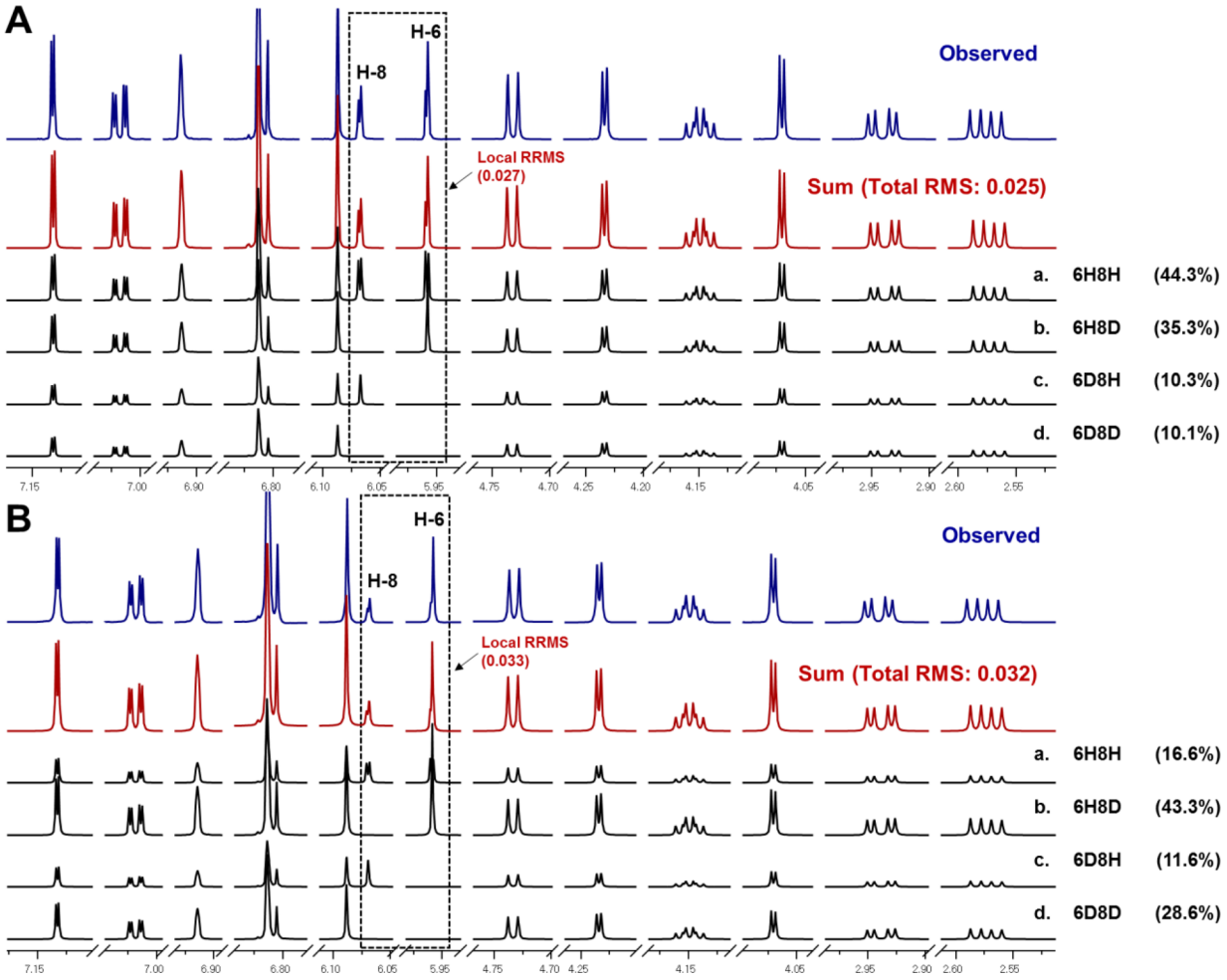


**Figure 5.** Simultaneous identification and molar ratios (in %) of the four isotopomers of **1** determined by HiFSA-qNMR. The sum (red) of the four intensity adjusted fingerprints is in excellent agreement with each experimental $^1$H NMR spectrum (observed, in blue; 900 MHz at 298 K). (A) and (B) are the $^1$H NMR spectra of **1** stored for 4 and 12 months, respectively, in $CD_3OD$ at −20 °C. The local RRMSs of the HiFSA fits are 0.027 (A) and 0.033 (B).

each carbon (C-6/8) triggered by the acidity of the C-5 and C-7 hydroxy groups.

To examine the H/D exchange effect, $^1$H NMR spectra of compound **1** were acquired at two different time points: 4 and 12 months following sample preparation and storage in $CD_3OD$ at −20 °C. A closer examination of the H-6 and H-8 resonances revealed that peak shapes and intensities were altered due to the presence of the deuterated species. H/D exchange in the A-ring can result in four possible species of **1**: 6H8H, 6H8D, 6D8H, and 6D8D. The residual H-6 of the D-ring also exhibited the same effect, as became evident by comparing peak areas. However, its exchange rate is relatively low as compared to those of H-6 and H-8 in the A-ring.

The proton coupled with deuterium (A-H-6 of 6H8D, A-H-8 of 6D8H) gave rise to apparent broad singlets, which are actual triplets with very small reduced couplings ($J_{H,D} = J_{H,H}/6.514$).[28] The initial $\delta_H$ values of H-6 and/or H-8 in the 6H8H, 6H8D, and 6D8H species were determined using the PERCH TLS module. In general, spectral deconvolution techniques have been used for quantification to identify heavily overlapped spectral signals.[36] However, the peak deconvolution approach can misguide spectral analysis by simply fitting whatever broad peaks it might take to mimic the experimental spectrum. It could be an artifact, which has no connection to the underlying spin system. To resolve this problem, HiFSA methodology was applied to fully interpret the overlapped $^1$H resonances of **1** as a mixture of all four isotopomers (A-ring 6H8H, 6H8D, 6D8H, and 6D8D). This involved simulation of the $^1$H NMR spectrum of each isotopomer and QMTLS iteration until the simulated matched the observed spectrum, and then the exact $\delta_H$ and $J$ values of each species were determined. The final local RRMSs for the region of H-6 and H-8 were 0.027 (4 months) and 0.033 (12 months), and, thus, below the general acceptance criterion of 0.1. The outcome enabled both recognition and, for the first time, even quantitation of the four isotopomeric H/D-species in the time-resolved study of these exchange phenomena. The molar ratios (%) of the four isotopomers of **1** were calculated after TLS iteration using the HiFSA-qHNMR method (Figure 5) based on the combined spectral parameters of all species, as follows: after 4 months, the molar ratios of 6H8H, 6H8D, 6D8H, and 6D8D were 44.3%, 35.3%, 10.3%, and 10.1%, respectively; after 12 months, the mixture consisted of 16.6%, 43.3%, 11.6%, and 28.6% of the isotopomers, respectively. From these results, different D exchange rates between A-H-6 and A-H-8 could be deduced as compared to the populations of each species; thus the exchange rate of H-8 is faster than that of H-6, which means the electron density at C-8 is greater than that of C-6 in **1**. Moreover, the C−D bond


DOI: 10.1021/acs.joc.5b01082
J. Org. Chem. 2015, 80, 7495−7507

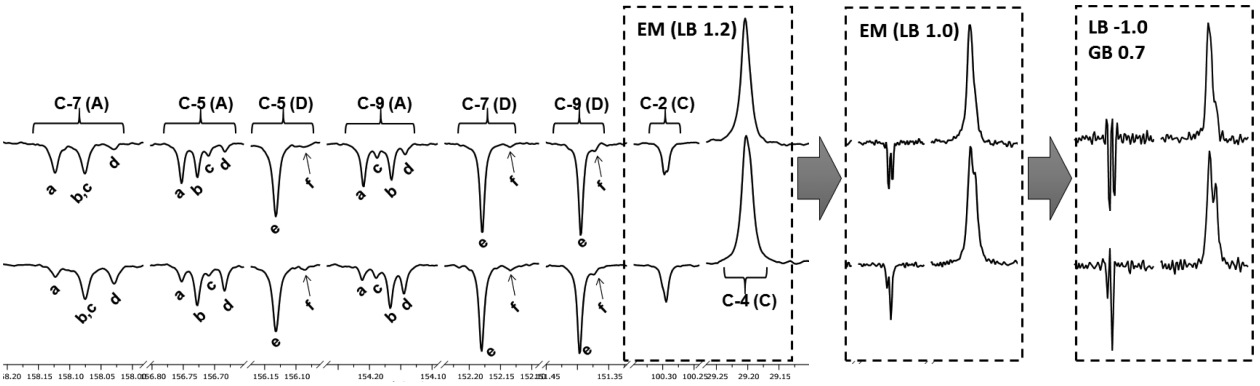


**Figure 6.** $^{13}$C DEPTQ-135 spectra of a sample of **1** ($CD_3OD$, 225 MHz, 298 K) stored in $CD_3OD$ at −20 °C for 4 (top) and 12 months (bottom). A-ring isotopomers: a = 6H8H, b = 6H8D, c = 6D8H, d = 6D8D. D-ring isotopomers: e = 6H, f = 6D.

has a higher bond energy than the C−H bond ($\Delta E$ = 4.8 kJ/mol),[37] and thus the population of deuterated species increases slightly with time.

The areas of the H/D isotopomer signals in the DEPTQ-135 $^{13}$C NMR spectra provide independent support for the populations calculated by HiFSA-qHNMR (Figure 6). The spectra even exhibited the small but characteristic four-bond deuterium SCS effects ($\Delta\delta_C$ = 5−10 ppb), but their detection required resolution enhanced spectra (Lorentzian−Gaussian window function; LB = −1.0, GB = 0.7). This observation underscores the need for careful 1D NMR processing: typical standard processing methods involve exponential multiplication with LB = 1.2 and, thereby, throw away meaningful information that is actually contained in the data. Notably, the resonances of the deuterated carbons often remain undetected in DEPTQ-135 spectra due to their long relaxation times, small NOE effects, and reduced signal-to-noise due to the multiplet nature of the signal.[34,38]

In addition to confirming the HiFSA-based $^1$H assignments of the H/D isotopomers, the $^{13}$C SCS effects exhibit a remarkably linear, additive behavior. The *ortho* and *para* deuterium $^{13}$C SCSs are 45 ± 3 and 23 ± 1 ppb, respectively. In the case of the 6D8D species, the additivity of these highly consistent SCSs is shown for the neighboring carbons (Figure 7). On the other hand, *meta* SCSs are below the line width of the $^{13}$C signals and, thus, remain undetected. Overall, both the $^1$H and the $^{13}$C chemical shift differences between the four isotopomeric species are very small, falling into the ppb-level chemical shift range, with $\Delta\delta_C$ values of 5−50 ppb and $\Delta\delta_H$ values of 0.5−1 ppb (S29,S30, Supporting Information). The $^1$H SCSs of C-6/-8 isotopomerism even reach into the upper ppt-level chemical shift range. The (sub)ppb-level chemical shift effects of PACs observed here extend beyond the subtle differential characteristics of the silybin case,[26] in both the $^1$H and the $^{13}$C domains, and provide further evidence that near identical structures can be distinguished by high-precision 1D NMR.

**Structure of the More Highly Oligomerized Bioactive PAC 3.** The trimeric procyanidin nature of **3** was evident from its molecular formula determined to be $C_{45}H_{36}O_{18}$ by HR-ESI−MS, which also suggested the presence of one A- and one B-type interflavanyl linkage. Restricted rotation around the B-type linkage of oligomeric PACs gives rise to the formation of atropisomers and excessive broadening of several NMR signals at room temperature (Figure 8).[4,12,39] Thus, the 1D and 2D NMR spectra of **3** were also obtained at low temperature (255 K) to improve spectral resolution and enhance the specificity of the assignments (S13−S17, Supporting Information). The $^{13}$C NMR chemical shifts at 255 K of **3** were extracted from the HSQC and HMBC spectra using the indirect projection method. NMR spectra acquired at 298 K were also interpreted (S18−S24, Supporting Information).

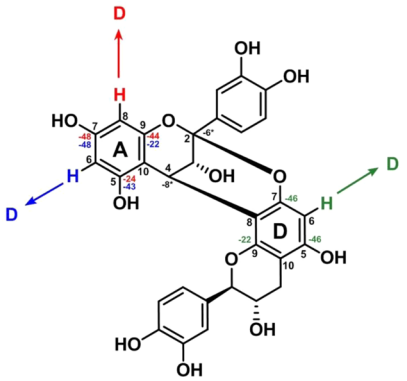


| position | A ring | | | D ring |
|---|---|---|---|---|
| | 6H8D | 6D8H | 6D8D | 6D |
| C5 | $^4J$ para -24 | $^2J$ ortho -43 | $^2J$ ortho + $^4J$ para -68 | $^2J$ ortho -46 |
| C7 | $^2J$ ortho -48 | $^2J$ ortho -48 | $^2J$ ortho + $^2J$ ortho -94 | $^2J$ ortho -46 |
| C9 | $^2J$ ortho -44 | $^4J$ para -22 | $^2J$ ortho + $^4J$ para -66 | $^4J$ para -22 |

**Figure 7.** Deuterium isotope SCS effects on the $^{13}$C chemical shifts (deuteration SCS, in ppb) of **1**, stored in $CD_3OD$ solution for 12 months. Asterisks (*) denote four-bond small SCS effects caused by deuterium exchange.

The $^1$H NMR spectrum of **3** exhibited the resonances for three AMX spin systems, indicating the presence of three 1,3,4-trisubstituted aromatic rings (B, E, and H). Additional resonances of an AX spin system at $\delta_H$ 4.12 (d, $J$ = 3.4 Hz, II-H-3) and 4.30 (d, $J$ = 3.4 Hz, II-H-4) were assigned to H-3 and H-4 of a doubly linked A-type PAC. The presence of a doubly linked structure was also supported by an acetal carbon resonance at $\delta_C$ 100.2 (II-C-2). The NOESY correlation observed between II-H-3 and III-H-6 indicated a 3,4-*trans* (F-ring) configured (*ent*-)epicatechin unit.[40,41] The $^1$H resonances at $\delta_H$ 4.70 (d, $J$ = 8.3 Hz, III-H-2), 4.15 (ddd, $J$ = 8.7, 8.3, 5.8 Hz, III-H-3), 3.01 (dd, $J$ = 16.3, 5.8 Hz, III-H-4a), and 2.57 (dd, $J$ = 16.3, 8.7 Hz, III-H-4b) also indicated an (*ent*-)catechin moiety to be the terminal unit of **3**. Broad $^1$H singlets assigned to H-2 and H-3 were indicative of a *cis* configured C-ring. Inclusion of the 2D NMR experiments (COSY, NOESY, HSQC, HMBC) allowed unambiguous assignment of all $^1$H


DOI: 10.1021/acs.joc.5b01082
J. Org. Chem. 2015, 80, 7495−7507

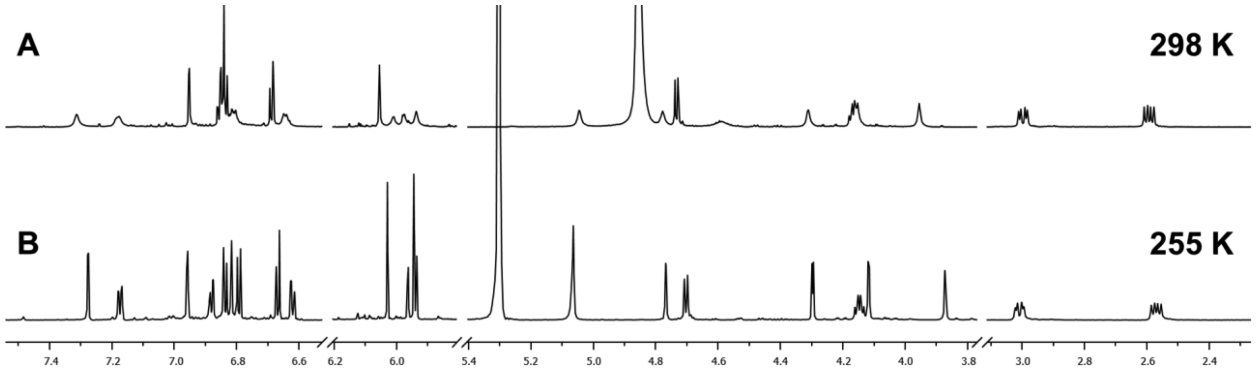


**Figure 8.** At 298 K (A; $CD_3OD$, 800 MHz), the $^1H$ NMR spectrum of **3** showed severe peak broadening for the signals from units I and II, which are immediately involved in the rotatable B-type interflavanyl bond, whereas the resonances of the remote unit III are practically unaffected by the rotameric dynamics. At 255 K (B), one greatly predominating atropisomer is frozen out, yielding a spectrum that is fully amenable to HiFSA and has only very minor signals of the higher energy rotamers.

NMR resonances and suggested that an A-type procyanidin dimer (units II and III) is linked to an epicatechin-like monomer (unit I) via a B-type interflavanyl bond. The HMBC spectrum proved the 4→8 interflavanyl linkage of units I and II via the cross-peaks from H-4 (C ring) to C-7, C-8, and C-9 (D ring).

The absolute configuration of **3** was determined by ECD in combination with NOE information from a 2D NOESY spectrum. The $\beta$-configurations at C-4 of the C- and F-rings were evident from the positive Cotton effect at 223 nm ($\Delta\varepsilon$ +43.87).[23] Notably, in the $^1H$ and $^{13}C$ NMR spectra of **3** acquired at 298 K, the subset of resonances belonging to unit III fully coincided with the signals from unit II of **1**, which was established independently as catechin, not *ent*-catechin. The absolute configurations at C-2 of the C-, F-, and I-rings were also confirmed by the ECD spectrum (S10, Supporting Information). It is known that flavan-3-ols with 2*R* (2$\alpha$) and 2*S* (2$\beta$) configuration show negative and positive Cotton effects, respectively, at 260−280 nm.[42] As compared to **1** ($\Delta\varepsilon$ = −11.49), the smaller amplitude of the negative Cotton effect in **3** ($\Delta\varepsilon$ = −5.15) at 270−280 nm suggested that the absolute configuration at C-2 of the C-ring was different from those of the F- and I-rings, whereas the C-2 configurations in the dimer **1** are identical to those in the dimeric subunits II+III of **3**.[43] These conclusions about the relative configuration of the unit I in **3** were confirmed by the 2D NOESY: correlations between H-2 and H-4 of the C-ring indicated that they are *cis* positioned to each other (Figure 9). The 2,3-*cis*-3,4-*cis* ABC-moiety of compound **3** is unique and exceptional among PAC molecules, as the axial C-3 hydroxy function has been described as directing the coupling process toward the formation of 2,3-*cis*-3,4-*trans* analogues.[44] Collectively, all analytical data of **3** are most compatible with the structure of the new trimeric PAC, *ent*-epicatechin-(4$\beta$→8)-epicatechin-(2$\beta$→*O*→7,4$\beta$→8)-catechin.

**HiFSA and Isotopomerism of 3.** Affirmation of the relative configuration of **3** came from the HiFSA profile[25,26] developed for **3** (Table 2), which led to the precise determination of the $^1H$ chemical shifts (0.1 ppb) and coupling constants (10 mHz). As described for **1**, the $^1H$ NMR spectrum of **3** also exhibited a residually unmatched region with a local RRMS value of 0.12. This slight nonfulfillment of the general HiFSA acceptance criterion ([R]RMS < 0.10) again reflected the H/D exchange in positions 6 and 8 of the A-ring, occurring during storage in $CD_3OD$. A resolution enhanced $^1H$ NMR

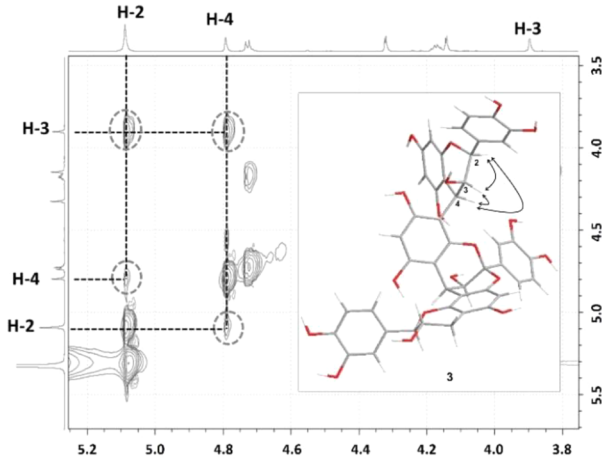


**Figure 9.** Key $^1H-^1H$ NOESY correlations (↔) of **3**.

spectrum of **3** stored at −20 °C for 2 months (Figure 10) clearly showed the presence of the D isotopomers.

To quantify the D isotopomers of **3**, simulated spectra of all four isotopomeric species were created and combined, as described for **1**. The population of each species was then calculated by HiFSA-qHNMR (Figure 11) to determine the molar ratio of these isotopomers as 40.9% 6H8H, 23.7% 6H8D, 18.9% 6D8H, and 16.5% 6D8D. In line with **1**, the D exchange rate of H-8 in **3** was also faster than that of H-6.

**Potential Connections between Differential A-Ring H−D Exchange, PAC Biosynthesis, and Dentin Biomodification?** Oligomeric or polymeric PACs are built by flavan-3-ols or other PAC precursors, which are products of several branches of the flavonoid pathway.[45] The polymerization of PACs is potentially mediated by carbocation structures, during which electrophilic C-4 carbocations condense with nucleophilic C-6 or C-8 positions of other flavan-3-ols (S25, Supporting Information).[46] In nature, both procyanidins (catechin and epicatechin constituent units) and prodelphinidins (gallocatechin and epigallocatechin constituent units) favor the C-4→C-8 linkage with a ratio of 3:1 (C-4→C-8:C-4→C-6). In contrast, the C-4→C-6 linkage is more stable than the C-4→C-8 linkage in 5-deoxy PACs.[46,47] The present achievement of quantifying isotopomers via HiFSA-qNMR and $^{13}C$ NMR led to the insight that H/D exchange occurs more rapidly at C-8 relative to C-6. This finding confirms that the


DOI: 10.1021/acs.joc.5b01082
J. Org. Chem. 2015, 80, 7495−7507

Table 2. $^1$H NMR Spectroscopic Data of 3[a,b]

| ring | no. | 3 $\delta_H$ ($J$, Hz) |
|---|---|---|
| unit I | | |
| C | 2 | 5.0647, d (0.99) |
| | 3 | 3.8726, dd (1.98, 0.99) |
| | 4 | 4.7681, d (1.98) |
| A | 6 | 5.9352, d (2.43)[d] |
| | 8 | 5.9633, d (2.43)[d] |
| B | 2′ | 6.8170, d (1.99) |
| | 5′ | 6.6671, d (8.20) |
| | 6′ | 6.6209, dd (8.20, 1.99) |
| unit II | | |
| F | 3 | 4.1182, d (3.37) |
| | 4 | 4.2974, d (3.37) |
| D | 6 | 5.9439, s |
| E | 2′ | 7.2763, dd (2.11, <0.10[c]) |
| | 5′ | 6.7926, dd (8.37, <0.10[c]) |
| | 6′ | 7.1738, dd (8.37, 2.11) |
| unit III | | |
| I | 2 | 4.7036, d (8.26) |
| | 3 | 4.1481, ddd (8.73, 8.26, 5.84) |
| | 4a | 3.0070, dd (−16.26, 5.84) |
| | 4b | 2.5702, dd (−16.26, 8.73) |
| G | 6 | 6.0288, s |
| H | 2′ | 6.9578, dd (2.03, <0.10[c]) |
| | 5′ | 6.8373, dd (8.12, <0.10[c]) |
| | 6′ | 6.8799, dd (8.12, 2.03) |

[a]Acquired in $CD_3OD$ at 800 MHz at 255 K. [b]The $\delta_H$ (in ppm) and $J$ (in Hz) values were generated via $^1$H iterative full spin analysis (HiFSA). [c]Very small couplings (0.03−0.08 Hz) detected by HiFSA and required for the overall fit. [d]Chemical shifts and coupling constants of nondeuterated species (6H8H).

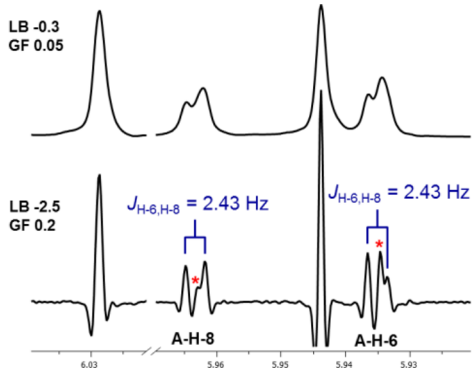


**Figure 10.** Lorentzian−Gaussian resolution enhancement (lower trace) of the $^1$H NMR spectrum uncovers the H/D isotopomeric composition of **3** after 2 months of storage at −20 °C in $CD_3OD$. In contrast, standard processing fails to reveal the actual multiplicity of the A-H-6 and A-H-8 signals (* denotes the signal of the monodeuterated isotopomer).

electron densities on C-8 are higher than those on C-6,[48] particularly in the upper PAC unit. These differences can be part of the explanation as to why preferences for C−C connection sites exist in the biosynthesis of PACs, and are in line with observed favored linkage sites in the naturally occurring molecules of this class.

As plant polyphenols are well-known to generate complexes with various types of proteins, the pronounced specificity of particular OPACs from certain plants to increase the biomechanical properties of dentin is remarkable. The present finding of the trimeric PAC, **3**, from pine bark, as the most potent single chemical with dentin biomodification activity known to date implies that relatively minor structural modifications of the polyphenols can lead to major changes in the bioactivity. As knowledge of the protein−PAC complexes is only starting to evolve,[49] the formulation of exact interaction mechanisms with specific intermolecular interactions remains a future task. However, the present observation of A-ring H−D exchange effects, which is upheld by the observed ppb-level SCS effects, is potentially important for achieving a broader understanding of how particular dentin-active PACs can cross-link the dentin protein matrix. It is known that the main interactions of PACs and collagen complexes are H-bonding between collagen carbonyl and the phenolic hydroxy groups.[50] Different acidities of 5-OH and 7-OH groups indicate both increased reactivity and a preference of bonding site(s) in PAC molecules. Moreover, high electron densities at C-6/C-8 suggest that, similar to the biosynthetic establishment of C−C linkages, the formation of covalent C−C bonds could be a possible mechanism of bonding between the peptidic collagen nanostructures and the PACs. This plausible mechanism applies in addition to, for example, H-bonding, $\pi$-stacking, and hydrophobic interactions.[50,51] Regardless of the exact mechanism, the chemical shifts ($\Delta\delta$) in ppb already provide evidence for subtle changes in structural properties, which translate into major differences in the ability of PACs to induce collagen cross-links inter-molecularly and inter-microfibrillarly, both occurring in nanometer-scale spaces.

**Dentin Biomechanical and Biostability Assay of PACs.** Compounds **1**−**3** were isolated from a fraction of pine extract that showed prominent dentin bioactivity. In a previous study, the effects of proanthocyanidin A1 (**1**) and A2 (**2**) on dentin biomechanics had been evaluated in a 3-point bending assay, together with the other commercially available PACs, proanthocyanidins B1, B2, and C1.[11] Along with the new trimeric PAC, **3**, the pine isolates **1** and **2** were tested again for comparison. Compound **3** showed significantly higher activity in both the dentin biomechanical and the biostability assays, superior to any other PACs tested previously (Figure 12). The superior dentin biomodification of **3** can be attributed to several factors: (i) The presence of a terminal catechin unit: PACs B1 and A1 both possess catechin terminal units, and both have higher activity in enhancing dentin modulus of elasticity than B2 and A2, which have epicatechin terminal units.[11] (ii) The trimeric nature of **3**: detailed biological profiling of the active fractions of pine and other plants (not shown) indicates that, in terms of the degree of polymerization (DP), the trimeric and tetrameric PACs hold the key to promote precisely high dentin biomodification abilities. (iii) Compound **3** apparently fulfills a favorable combination of DP, interflavanyl linkage type, conformational and spatial properties, and the presence of catechin as terminal monomeric unit to be able to exhibit a profound enhancement of dentin matrix biomechanics. Moreover, compound **3** significantly lowered the biodegradation rate of collagen, suggesting that **3** might inhibit enzyme-induced degradation.[52] These results also support the conclusion that the PAC−collagen complexes likely involve strong bonds, such as stabilized hydrogen bonds and/or irreversible covalent bonds, leading to high resistance against proteolytic dentin degradation.


DOI: 10.1021/acs.joc.5b01082
J. Org. Chem. 2015, 80, 7495−7507

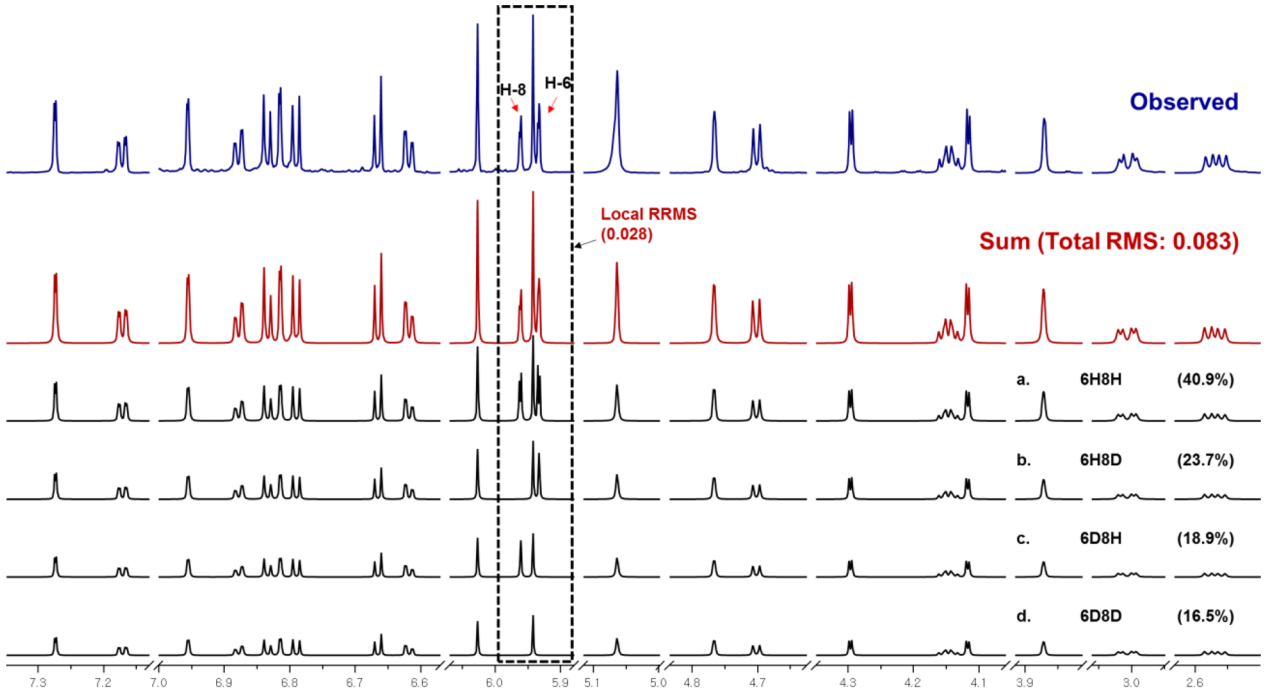


**Figure 11.** Molar ratios of the four isotopomeric species (%) in **3** generated after 2 months of storage in $CD_3OD$ at −20 °C were calculated by HiFSA-qNMR. The sum of the four intensities adjusted fingerprints (sum, in red) is in full agreement with the experimental low-temperature $^1H$ NMR spectrum (observed, in blue, 800 MHz at 255 K, $CD_3OD$). The local RRMS for the $\delta_H$ 5.9−6.0 ppm region was 0.028.

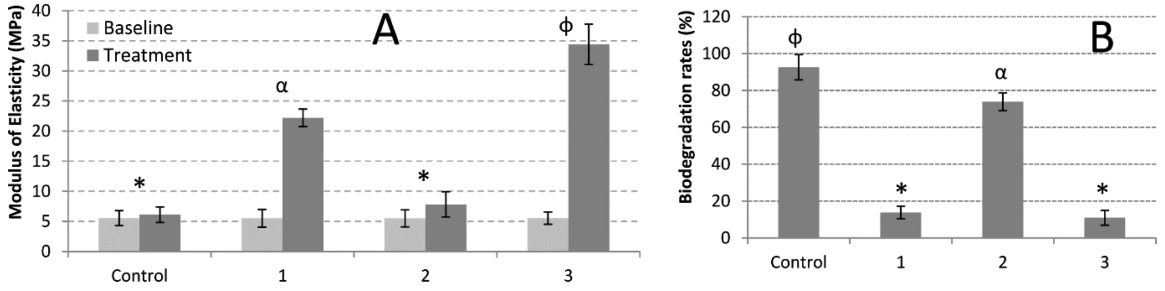


**Figure 12.** Mean and standard deviation of the apparent modulus of elasticity (A, in MPa) and biodegradation rates (B, in %) of dentin beams treated with **1**−**3**. Different symbols depict statistical differences among groups ($p < 0.05$).

In the present study, the H/D exchange of H-8 (A-ring) of **3** occurred relatively fast (40% deuteration in 2 months at −20 °C) as compared to the other compounds (**1**, 45% deuteration in 4 months, **2**, <5% deuteration in 4 months). Although other factors such as concentration and pH were not controlled, these differences nurture the hypothesis that a relationship exists between the dentin bioactivity (bonding between collagen and [O]PACs) and the A-ring electron density of these polyphenols.

## CONCLUSIONS

Despite many earlier efforts, and even though advanced analytical methodology has become available, the structural characterization of trimeric and higher oligomerized PACs remains challenging. This is largely due to the intrinsic structural characteristics of these natural polyphenols: they are oligomers of near-identical monomers; OPACs show abundant occurrence of atropisomeric forms, leading to dynamic challenges, for example, in NMR spectroscopy; in plants, as numerous near-identical congeners are produced, individual OPACs are difficult to purify. As most analytical approaches that have investigated bioactive OPACs have applied degradative methods and relied largely on the identification of the monomeric units, information about the physicochemical properties of intact bioactive oligomers is missing, and often no material is left for biological evaluation.

To address these challenges in the study of OPACs that are potent dentin biomodifiers, the present study purified the free phenolic forms of **1**−**3**, and elucidated the structures of the intact oligomers, ab initio, by spectroscopic methods (1/2D NMR, MS, ECD) without degradation. Employing low temperature NMR as well as QM-based HiFSA methodology addressed atropisomerism and H/D isotopomerism. Moreover, the combined use of exhaustive $^1H$ NMR spectroscopic interpretation via HiFSA and ECD data enabled the assignment of the absolute configuration of all monomeric building blocks in the oligomers **1**−**3**. Considering that, to date, underivatized trimeric or higher oligomerized PACs have not been amenable to X-ray crystallography, the assignment of absolute stereochemistry without the need for degradation provides an important piece of information: the stereochemistry of the [*epi*-]/[*ent*-]catechin subunits predictably has a major impact on the overall shape of the oligomers and, thus, on their biological activity.



DOI: 10.1021/acs.joc.5b01082
*J. Org. Chem.* 2015, 80, 7495−7507

The HiFSA approach, aided by $^{13}C$ NMR, enabled a new level of interpretation of the $^{1}H$ NMR spectra of the OPACs. This led to the recognition of several diagnostic effects: (i) occurrence of higher order spin coupling of aromatic protons, leading to largely different and potentially confusing spectroscopic fingerprints of otherwise identical monomeric units; (ii) presence of $^{4}J$ long-range coupling that connects the B- and C-rings of the catechin units in the dimers **1** and **2**, but interestingly not in the trimer, **3**; (iii) prominent and site-specific H/D exchange at C-8 and C-6 of the A-ring, producing a mixture of isotopomers in deuterated solution at −20 °C; and (iv) the occurrence of subtle, but structurally significant, chemical shift effects at the ppb-level (SCS; 0.3 ppb in $^{1}H$, 6 ppb in $^{13}C$), which reflect the H/D exchange reactions and individual C−H acidities. The first successful generation of a HiFSA profile of a trimeric PAC also enabled the precise quantification of each isotopomeric species via HiFSA-qHNMR.

Collectively, these data not only help to explain why biosynthetic linkages in OPACs occur primarily via C-8 and, to a lesser degree, C-6, but also nurture the conclusion that a connection exists between the observed chemical, spectroscopic, and biological phenomena, all occurring at the nano level. As a single chemical entity, the new trimeric PAC, **3**, is the most potent dentin biomodification agent known to date, capable of increasing dentin modulus of elasticity by 7-fold. The experiments demonstrate that **3** must have just the right molecular shape to cross-link the 1.3−4.5 nm wide spaces in the peptidic backbone of teeth with high binding specificity, producing an increase in dentin modulus of elasticity at the nano scale. This makes the present study an instance of (dental) nano meeting (chemical) nano: mining the highly information-rich 1D $^{1}H$ and $^{13}C$ NMR spectra by HiFSA and resolution-enhanced processing, aided by chiroptical methods, provides a new avenue for mapping the exact 3D structures of OPACs, including the determination of their absolute stereochemistry, and unveils the (re)active properties of these complex polyphenols. This bodes well on their characterization in free phenolic form, which is a prerequisite for their biological evaluation and has potential to advance the nature of restorative dentistry in the future.

## EXPERIMENTAL SECTION

**General Experimental Procedures.** Optical rotation and ECD spectra were measured at 25 °C using methanol. Mass spectrometry was carried out with an IT-TOF hybrid mass spectrometer. Standards compounds (proanthocyanidin A1 and A2) were used as received from commercial supplier. Silica gel (230−400 mesh) was used for column chromatography. TLC was performed on SIL G/UV254 (silica gel 60, 0.20 mm layer thickness) with visualization under UV light (254 and 365 nm) and vanillin-sulfuric acid reagent spray followed by heating (120 °C, 5 min). Preparative HPLC was carried out using a YMC-Pack ODS-AQ (250 × 10 mm, S-5, 12 nm) column equipped with a photodiode array detector.

**Plant Material, Extraction, and Isolation.** Extract powder of the inner bark of *P. massoniana* was purchased from Xi'an Chukang Biotechnology in China in 2012 (no. PB120212). The extract (100 g) was separated by silica gel flash column chromatography (10 × 20 cm) using dichloromethane and 1% water in methanol (98:2 to 50:50) as a gradient solvent system to afford 42 fractions (F01−F42). Subfraction F16 (4.0 g), eluted with dichloromethane and 1% water in methanol (80:20), was further fractionated by silica gel column chromatography (3 × 40 cm) using a $CHCl_3$−MeOH−water gradient (90:10:1 to 70:30:1) to give 20 subfractions (F16.01−F16.20). Subfraction F16.08 (200 mg) was purified by semipreparative HPLC using a $C_{18}$ reversed-phase column with an isocratic solvent system of acetonitrile−0.1% formic acid in water (20:80) to provide compounds **1** (15.0 mg) and **2** (7.0 mg). Compound **3** (15.0 mg) was obtained from subfraction F16.10 (150 mg) by separation with semipreparative HPLC equipped with a $C_{18}$ reversed-phase column, using an isocratic solvent system of acetonitrile−0.1% formic acid in water (20:80).

*Epicatechin-(2β→O→7,4β→8)-catechin (Proanthocyanidin A1, **1**).* Light brown amorphous solid; ECD (MeOH) $\lambda_{max}$ ($\Delta\varepsilon$) = 223 (+28.58), 272 (−11.49) nm; $^{1}H$ and $^{13}C$ NNMR, see Table 1; HRESIMS $[M + H]^+$ $m/z$ 577.1371 (calcd for $C_{30}H_{25}O_{12}$, 577.1346).

*Epicatechin-(2β→O→7,4β→8)-epicatechin (Proanthocyanidin A2, **2**).* Light brown amorphous solid; ECD (MeOH) $\lambda_{max}$ ($\Delta\varepsilon$) = 223 (+33.63), 272 (−6.28) nm; $^{1}H$ and $^{13}C$ NMR, see Table 1; HRESIMS $[M + H]^+$ $m/z$ 577.1320 (calcd for $C_{30}H_{25}O_{12}$, 577.1346).

*ent-Epicatechin-(4β→8)-epicatechin-(2β→O→7,4β→8)-catechin (**3**).* Light brown amorphous solid; $[\alpha]^{25}_{D}$ +86.60 (*c* 0.11, MeOH); ECD (MeOH) $\lambda_{max}$ ($\Delta\varepsilon$) = 223 (+43.87), 274 (−5.15) nm; H NMR at 255 K, see Table 2; $^{1}H$ and $^{13}C$ NMR at 298 K, see Supporting Information S24; HRESIMS $[M + H]^+$ $m/z$ 865.2015 (calcd for $C_{45}H_{37}O_{18}$, 865.1980).

**NMR Spectroscopy.** RT (298 K) NMR measurements were performed on 600 and 900 MHz spectrometers equipped with TXI and TCI cryoprobes, respectively. Low-temperature NMR (255 K) spectra were acquired on an 800 MHz spectrometer equipped with a TXI RT probe. All NMR spectra were obtained using methanol-$d_4$ as the solvent. NMR samples, 5.53 mg (**1**), 1.10 mg (**2**), and 7.76 mg (**3**), respectively, were prepared in 3 mm tubes with 170 μL of $CD_3OD$. The chemical shifts of the residual solvent signals at $\delta_H$ 3.3100 and $\delta_C$ 49.000 were used as the chemical shift reference. The $^{1}H$ NMR data for HiFSA were processed using a Lorentzian−Gaussian window function (line broadening = −0.3, Gaussian factor = 0.05) prior to Fourier transformation.

**Computer-Aided NMR Spectral Analysis.** The $^{1}H$ iterative full spin analysis (HiFSA) was performed by PERCH NMR software package (ver. 2013.1) as described previously.[53,54] The optimized spectral parameters were saved as PERCH parameters text files (*.pms). Four and two decimal places for $\delta_H$ and $J$ values, respectively, were considered significant (S26−S28, Supporting Information).

For the examination of H/D isotopomer mixtures of **1**−**3**, the simulated $^{1}H$ NMR spectra of four isotopomers (6H8H, 6H8D, 6D8H, and 6D8D) were generated using the PERCH spectral parameter editor. The optimized NMR parameters of each isotopomer were combined into a single *.pms file and imported into the PMS module. The four $^{1}H$ NMR profiles of the isotopomers were simultaneously fitted to the experimental spectra using QMTLS iteration. The optimized coupling constants of each isotopomer were fixed to avoid distortion of the signals during the iteration, yielding the relative molar populations (mol %) of each species (S29−S31, Supporting Information). The standard deviation of the relative molar populations obtained from multiple iterations with different optimization settings for the line-shape (individual line-widths for each spin-particle, overall Gaussian/Lorentzian distribution, and dispersion) was 0.1−0.5%.

**Dentin Biomechanical and Biostability Assay.** Human molars were used for the dentin biomechanical assay after approval by the Institutional Review Board Committee of the University of Illinois at Chicago (protocol no. 2011-0312). The teeth were cut into 0.5 × 1.7 × 6.0 ($H \times W \times L$) mm sized dentin beams, demineralized using phosphoric acid, treated with sample diluted in 20 mM HEPES buffer pH 7.4, and apparent modulus of elasticity (in MPa) was measured using a universal testing machine. Buffer-only treated dentin beams were used as controls as described previously.[2,55] Compounds **1**−**3** were tested at 0.65% w/v concentration for 1 h. Biostability assays were followed by dentin biomechanical assays with the same dentin specimens incubated in collagenase (100 μg/mL *Clostridium histolyticum* bacterial collagenase) at 37 °C as previously described.[55] The effects of **1**−**3** were statistically evaluated by two-way ANOVA and Tukey's post hoc tests ($\alpha$ = 0.05).



DOI: 10.1021/acs.joc.5b01082
J. Org. Chem. 2015, 80, 7495−7507

## ■ ASSOCIATED CONTENT

### Supporting Information

$^1$H NMR spectroscopic comparison between standard compounds (PACs A1 and A2) and compounds **1**/**2**; ECD spectra; 1D/2D $^1$H and $^{13}$C NMR spectra, including raw 1D NMR data (FIDs); qNMR profiles including calculation spreadsheets; PERCH-generated *.pms text files (spectral parameters) of compounds **1**−**3**; $^1$H and $^{13}$C NMR spectroscopic data table of compound **3** at 298 K; schemes regarding PACs biosynthesis and deuterium exchange; and animated graphic showing the higher order progression of the AMX spin system described in Figure 3. The Supporting Information is available free of charge on the ACS Publications website at DOI: 10.1021/acs.joc.5b01082.

## ■ AUTHOR INFORMATION

### Corresponding Author

*E-mail: gfp@uic.edu.

### Notes

The authors declare the following competing financial interest(s): M.N. is an employee at Perch Solutions Ltd. The other authors declare no competing financial interest.

## ■ ACKNOWLEDGMENTS

The research at the University of Illinois at Chicago was funded by grant R01 DE021040 from NIDCR/NIH. The construction of the UIC CSB and the purchase of the 800 and 900 MHz NMR spectrometers was generously funded by a grant to Dr. Peter Gettins from NIGMS Grant no. P41 GM068944. We appreciate the very helpful and detailed comments on the (stereo)chemistry of proanthocyanidins provided by one of the reviewers.

## ■ REFERENCES

(1) Bedran-Russo, A. K.; Pashley, D. H.; Agee, K.; Drummond, J. L.; Miescke, K. J. *J. Biomed. Mater. Res., Part B* **2008**, *86*, 330−334.
(2) Aguiar, T. R.; Vidal, C. M. P.; Phansalkar, R. S.; Todorova, I.; Napolitano, J. G.; McAlpine, J. B.; Chen, S. N.; Pauli, G. F.; Bedran-Russo, A. K. *J. Dent. Res.* **2014**, *93*, 417−422.
(3) Hemingway, R. W.; Foo, L. Y.; Porter, L. J. *J. Chem. Soc., Perkin Trans. 1* **1982**, 1209−1216.
(4) Phansalkar, R. S.; Nam, J.-W.; Chen, S.-N.; McAlpine, J. B.; Napolitano, J. G.; Leme, A.; Vidal, C. M. P.; Aguiar, T.; Bedran Russo, A. K.; Pauli, G. F. *Fitoterapia* **2015**, *101*, 169−178.
(5) Bedran-Russo, A. K.; Pauli, G. F.; Chen, S.-N.; McAlpine, J.; Castellan, C. S.; Phansalkar, R. S.; Aguiar, T. R.; Vidal, C. M. P.; Napolitano, J. G.; Nam, J.-W.; Leme, A. A. *Dent. Mater.* **2014**, *30*, 62−76.
(6) Wang, X.-H.; Huang, L.-L.; Yu, T.-T.; Zhu, J.-H.; Shen, B.; Zhang, Y.; Wang, H.-Z.; Gao, S. *Phytother. Res.* **2013**, *27*, 869−876.
(7) Li, X.; Yang, X.; Cai, Y.; Qin, H.; Wang, L.; Wang, Y.; Huang, Y.; Wang, X.; Yan, S.; Wang, L.; Zhao, X.; Li, W.; Li, S.; Chen, J.; Wu, Y. *Molecules* **2011**, *16*, 6721−6731.
(8) Yamakoshi, J.; Tokutake, S.; Kikuchi, M.; Kubota, Y.; Konishi, H.; Mitsuoka, T. *Microb. Ecol. Health Dis.* **2001**, *13*, 25−31.
(9) Fletcher, M. H.; Jennings, M. C.; Wuest, W. M. *Tetrahedron* **2014**, *70*, 6373−6383.
(10) Huang, S.; Yang, N.; Liu, Y.; Gao, J.; Huang, T.; Hu, L.; Zhao, J.; Li, Y.; Li, C.; Zhang, X. *Int. J. Mol. Med.* **2012**, *30*, 1410−1416.
(11) Vidal, C. M. P.; Leme, A. A.; Aguiar, T. R.; Phansalkar, R.; Nam, J.-W.; Bisson, J.; McAlpine, J. B.; Chen, S.-N.; Pauli, G. F.; Bedran-Russo, A. K. *Langmuir* **2014**, *30*, 14887−14893.
(12) Fletcher, A. C.; Porter, L. J.; Haslam, E.; Gupta, R. K. *J. Chem. Soc., Perkin Trans. 1* **1977**, 1628−1637.
(13) Torres, J. L.; Lozano, C.; Julià, L.; Sánchez-Baeza, F. J.; Anglada, J. M.; Centelles, J. J.; Cascante, M. *Bioorg. Med. Chem.* **2002**, *10*, 2497−2509.
(14) Jordheim, M.; Fossen, T.; Songstad, J.; Andersen, Ø. M. *J. Agric. Food Chem.* **2007**, *55*, 8261−8268.
(15) Pedersen, A. T.; Andersen, M.; Aksnes, D. W.; Nerdal, W. *Magn. Reson. Chem.* **1993**, *31*, 972−976.
(16) Pauli, G. F.; Chen, S.-N.; Lankin, D. C.; Bisson, J.; Case, R.; Chadwick, L. R. d.; Gödecke, T.; Inui, T.; Krunic, A.; Jaki, B. U.; McAlpine, J. B.; Mo, S.; Napolitano, J. G.; Orjala, J.; Lehtivarjo, J.; Korhonen, S.-P.; Niemitz, M. *J. Nat. Prod.* **2014**, *77*, 1473−1487.
(17) Boudesocque, L.; Dorat, J.; Pothier, J.; Gueiffier, A.; Enguehard-Gueiffier, C. *Food Chem.* **2013**, *139*, 866−871.
(18) Pauli, G. F.; Chen, S.-N.; Simmler, C.; Lankin, D. C.; Gödecke, T.; Jaki, B. U.; Friesen, J. B.; McAlpine, J. B.; Napolitano, J. G. *J. Med. Chem.* **2014**, *57*, 9220−9231.
(19) Appeldoorn, M. M.; Sanders, M.; Vincken, J.-P.; Cheynier, V.; Le Guerneve, C.; Hollman, P. C. H.; Gruppen, H. *Food Chem.* **2009**, *117*, 713−720.
(20) Lou, H.; Yamazaki, Y.; Sasaki, T.; Uchida, M.; Tanaka, H.; Oka, S. *Phytochemistry* **1999**, *51*, 297−308.
(21) Zhang, H.; Yerigui; Yang, Y.; Ma, C. *J. Agric. Food Chem.* **2013**, *61*, 8814−8820.
(22) Li, X.; Jin, H.; Yang, M.; Chen, G.; Shen, Y.; Zhang, W. *Chem. Nat. Compd.* **2010**, *46*, 106−108.
(23) Botha, J. J.; Young, D. A.; Ferreira, D.; Roux, D. G. *J. Chem. Soc., Perkin Trans. 1* **1981**, 1213−1219.
(24) Ding, Y.; Li, X.-C.; Ferreira, D. *J. Nat. Prod.* **2010**, *73*, 435−440.
(25) Napolitano, J. G.; Godecke, T.; Rodriguez-Brasco, M. F.; Jaki, B. U.; Chen, S.-N.; Lankin, D. C.; Pauli, G. F. *J. Nat. Prod.* **2012**, *75*, 238−248.
(26) Napolitano, J. G.; Lankin, D. C.; Graf, T. N.; Friesen, J. B.; Chen, S.-N.; McAlpine, J. B.; Oberlies, N. H.; Pauli, G. F. *J. Org. Chem.* **2013**, *78*, 2827−2839.
(27) Barfield, M.; Chakrabarti, B. *Chem. Rev.* **1969**, *69*, 757−778.
(28) Friebolin, H. *Basic One- and Two-Dimensional NMR Spectroscopy*, 5th ed.; Wiley-VCH: Weinheim, 2011.
(29) Musher, J. I.; Corey, E. J. *Tetrahedron* **1962**, *18*, 791−809.
(30) Pauli, G. F. *J. Nat. Prod.* **2000**, *63*, 834−838.
(31) Liimatainen, J.; Karonen, M.; Sinkkonen, J. *Phytochemistry* **2012**, *76*, 178−183.
(32) Tarascou, I.; Ducasse, M.-A.; Dufourc, E. J.; Moskau, D.; Fouquet, E.; Laguerre, M.; Pianet, I. *Magn. Reson. Chem.* **2007**, *45*, 157−166.
(33) Tarascou, I.; Barathieu, K.; Simon, C.; Ducasse, M.-A.; Andre, Y.; Fouquet, E.; Dufourc, E. J.; de Freitas, V.; Laguerre, M.; Pianet, I. *Magn. Reson. Chem.* **2006**, *44*, 868−880.
(34) Faizi, S.; Siddiqi, H.; Naz, A.; Bano, S.; Lubna. *Helv. Chim. Acta* **2010**, *93*, 466−481.
(35) Mehr, S. H. M.; Bishop, S.; MacLachlan, M. J.; Fukuyama, K.; Lelj, F. *J. Org. Chem.* **2015**, *80*, 5144−5150.
(36) Pauli, G. F.; Gödecke, T.; Jaki, B. U.; Lankin, D. C. *J. Nat. Prod.* **2012**, *75*, 834−851.
(37) Dill, K.; Bromberg, S. *Molecular Driving Forces: Statistical Thermodynamics in Biology, Chemistry, Physics, and Nanoscience*, 2nd ed.; Garland Science: New York, 2011.
(38) Gribble, G. W.; Nelson, R. B.; Johnson, J. L.; Levy, G. C. *J. Org. Chem.* **1975**, *40*, 3720−3725.
(39) Shoji, T.; Mutsuga, M.; Nakamura, T.; Kanda, T.; Akiyama, H.; Goda, Y. *J. Agric. Food Chem.* **2003**, *51*, 3806−3813.
(40) Cronje, A.; Burger, J. F. W.; Vincent Brandt, E.; Kolodziej, H.; Ferreira, D. *Tetrahedron Lett.* **1990**, *31*, 3789−3792.
(41) Cronje, A.; Steynberg, J. P.; Brandt, E. V.; Young, D. A.; Ferreira, D. *J. Chem. Soc., Perkin Trans. 1* **1993**, 2467−2477.
(42) Slade, D.; Ferreira, D.; Marais, J. P. J. *Phytochemistry* **2005**, *66*, 2177−2215.
(43) Lee, I.-S.; Yu, S. Y.; Jung, S.-H.; Lee, Y.-R.; Lee, Y. M.; Kim, J.-H.; Sun, H.; Kim, J. S. *J. Nat. Prod.* **2013**, *76*, 1881−1888.



DOI: 10.1021/acs.joc.5b01082
*J. Org. Chem.* 2015, 80, 7495−7507

(44) Coetzee, J.; Malan, E.; Ferreira, D. *Tetrahedron* **1999**, *55*, 9999−10004.
(45) Xie, D. Y.; Dixon, R. a. *Phytochemistry* **2005**, *66*, 2127−2144.
(46) He, F.; Pan, Q. H.; Shi, Y.; Duan, C. Q. *Molecules* **2008**, *13*, 2674−2703.
(47) De Bruyne, T.; Pieters, L.; Deelstra, H.; Vlietinck, A. *Biochem. Syst. Ecol.* **1999**, *27*, 445−459.
(48) Elliott, R. J.; Sackwild, V.; Richards, W. G. *J. Mol. Struct.: THEOCHEM* **1982**, *3*, 301−314.
(49) Ozdal, T.; Capanoglu, E.; Altay, F. *Food Res. Int.* **2013**, *51*, 954−970.
(50) Han, B.; Jaurequi, J.; Tang, B. W.; Nimni, M. E. *J. Biomed. Mater. Res.* **2003**, *65*, 118−124.
(51) Hatano, T.; Hemingway, R. W. *Chem. Commun.* **1996**, 2537−2538.
(52) Jackson, J. K.; Zhao, J.; Wong, W.; Burt, H. M. *J. Mater. Sci.: Mater. Med.* **2010**, *21*, 1435−1443.
(53) Napolitano, J. G.; Lankin, D. C.; Chen, S.-N.; Pauli, G. F. *Magn. Reson. Chem.* **2012**, *50*, 569−575.
(54) Napolitano, J. G.; Lankin, D. C.; McAlpine, J. B.; Niemitz, M.; Korhonen, S.-P.; Chen, S.-N.; Pauli, G. F. *J. Org. Chem.* **2013**, *78*, 9963−9968.
(55) Vidal, C. M. P.; Aguiar, T. R.; Phansalkar, R.; McAlpine, J. B.; Napolitano, J. G.; Chen, S.-N.; Araujo, L. S. N.; Pauli, G. F.; Bedran-Russo, A. K. *Acta Biomater.* **2014**, *10*, 3288−3294.



DOI: 10.1021/acs.joc.5b01082
*J. Org. Chem.* 2015, 80, 7495−7507